STIMULATED LIGHT SCATTERING IN GASEOUS Ar, O_2, AND Ar-O_2 MIXTURES

CHIMEI JAMES HSU

15066

STIMULATED LIGHT SCATTERING IN GASEOUS Ar, O_2, AND Ar-O_2 MIXTURES

by

Chimei James Hsu

Submitted in partial fulfilment
of the requirements for the degree of Master of Science
Memorial University of Newfoundland

March, 1971

TABLE OF CONTENTS

ABSTRACT

The backscattered light from pure argon and from argon-oxygen mixtures at ambient temperature was investigated using a giant-pulse ruby laser. The gas samples at pressures in the range of 400 psi to 5000 psi were irradiated by light at λ 6943Å, whose peak power was approximately 100 MW with temporal pulse width of 20 ns. When the backscattered light was analyzed by means of a Fabry-Perot interferometer, its frequency profile led to a nonlinear scattering phenomenon resembling stimulated thermal Rayleigh scattering (STRS) in absorbing gases. In the course of investigation, it was found that the presence of minute concentration of oxygen impurity in argon produced a pronounced effect on the intensity of this scattered light. The scattering is positively identified as STRS based on the following experimental features in conjunction with a modified Gray-Herman theory on STRS:

(1) The frequency shift of the scattered light is typically 0.01 cm^{-1} to the higher frequency side.

(2) As the density of pure argon gas is increased, the threshold power, ${}^{0}P_{th}$, decreases following the relationship which is consistant with the modified theory,

$$ {}^{0}P_{th} \propto \frac{1}{\sqrt{\rho_0}} \left(1 + \frac{\rho_n}{\rho_0}\right) \quad , $$

where ρ_0 is the argon gas density and ρ_n is a constant.

(3) When the threshold power, P_{th}, for an argon sample with a fixed oxygen impurity concentration is compared with that for pure

argon at the same density, the following phenomenological relationship is derived:

$$ {}^{0}P_{th}^{2}/P_{th}^{2} = (1 - Br) \quad , $$

where B is a constant and r the percent concentration of oxygen in the sample.

In the present modified theory, the existance of laser-induced plasma in the gas sample and the presence of oxygen molecules in the argon medium were taken into consideration.

Stimulated Brillouin scattering (SBS) in pure argon and in pure oxygen gases was also investigated as a function of density. The experimental determination of Brillouin shifts in these gases revealed a remarkable fact that the values obtained from the "higher order" SBS lines seem to give sets of "smooth" hypersonic velocities while those obtained from the first SBS shifts show unusually large fluctuations outside the estimated experimental error. This fluctuation may be attributable to the initial laser-induced disturbance in the gas medium which has a short time constant and, consequently, this disturbance contributes little to the recurring SBS components.

CHAPTER I

INTRODUCTION

Since the early days of spectroscopy, scattering of light in fluid medium has long been considered as an effective source of information with regard to the thermodynamic properties of the medium as well as the intra-molecular structure of its constituents. Among various aspects of light scattering, the frequency profile of the scattered light in the neighbourhood of the incident light frequency, which is known as the Brillouin-Rayleigh triplet[1], has recently become a subject of extensive investigation with the advent of laser which provided highly monochromatic light beams. The main features of this triplet are an unshifted central Rayleigh component and both Stokes-shifted and anti-Stokes-shifted Brillouin components. Adiabatic density fluctuations which correspond to the acoustic waves in the medium contribute to the Brillouin components, while the entropy fluctuations ("sharp" Rayleigh peak) and the anisotropy fluctuations (Rayleigh wing) contribute to the central component. The frequency shifts of the two Brillouin components from the central Rayleigh component correspond to the Doppler shift of the incident light by the thermal hypersonic waves present in the medium, which are given by

$$\omega_B = \pm 2n \frac{c_0}{c} \omega_L \operatorname{Sin} \frac{\theta}{2} \quad . \tag{1-1}$$

Here n, θ, and c_0 are the refractive index of the medium, the scattering

angle and hypersonic velocity, respectively; ω_L and c are frequency of the incident light and the velocity of light in vacuum, respectively. The positive sign refers to the Stokes Brillouin component and the negative sign to the anti-Stokes Brillouin component. It is noted that ω_B is equal to the frequency of the hypersonic waves producing the Brillouin doublet.

When a giant-pulse laser is used as a light source, the effects of the incident light field on the dielectric constant of the medium become important. This dependence of dielectric constant of the medium on the incident light field, on the other hand, can be easily neglected when a less intense light source is used. Change in the dielectric constant of the medium in an intense giant-pulse laser field gives rise to the growth of the intensity of the scattered field intensity at certain frequency or frequencies, producing the stimulated scattered light. Intensity of the stimulated scattered light, I_{stim}, is given by $I_{stim} = I_0 \exp\{GL\}$ where I_0 is the intensity of non-stimulated light present in the medium and analogous to noise signals in an electronic amplifier system; G is a gain function and L is the interaction length. The gain function G is usually dependent upon material parameters of the medium and laser field parameters, such as intensity and frequency.

There are several striking features which serve to identify the stimulated scattering:

(1) There exists a minimum input laser power level above which the stimulated process can occur. Existence of this power threshold is attributable to the lossy character of the medium; the

gain must be large enough to overcome this loss before I_{stim} becomes appreciable.

(2) So-called "gain narrowing" is also observable because of the exponential dependence of I_{stim}, namely, the half-intensity width of I_{stim} is considerably smaller than that of I_0.

(3) In general, the gain function has maximum values for more than one scattered component, but usually only one component corresponding to the frequency at which the gain has the largest value is observed. This is indicative of competition between two or more stimulated effects simultaneously present.

(4) As input laser power is increased above a certain level, the intensity of a stimulated component is often observed to stay stationary; in other words, saturation can take place in a stimulated process.

A number of stimulated effects, some corresponding to normal or "spontaneous" light scattering and some entirely new, have been observed in many solids, liquids, and gases. Examples are stimulated Raman scattering (SRS), stimulated Brillouin scattering (SBS), stimulated Rayleigh Wing scattering (SRWS), optical frequency mixing, and harmonic frequency generations.

Stimulated Brillouin Scattering

Since the first observation of stimulated Brillouin scattering in liquid by Garmire and Townes[2], there have been many reports on observations of SBS in a number of solids, liquids and gases[3],[4]. The frequency shift of the scattered light in SBS corresponds well with

that of the spontaneous Brillouin scattering at the scattering angle of 180^{o}. Accordingly, the hypersonic velocity in the medium, which may also be estimated from the Brillouin shift, ω_B, in SBS in conjunction with Eq. (1-1), can now be rewritten as:

$$C_0 = \frac{c}{2n\omega_L} |\omega_B| \quad , \tag{1-2}$$

where the nomenclatures used are the same as those in Eq. (1-1). For SBS, only the Stokes Brillouin component has been experimentally observed. It has been carried out theoretically that the SBS gain for the Stokes component is positive, while that for the anti-Stokes component is negative; the results thus explain the absence of the anti-Stokes component in SBS. Occasionally, however, anti-Stokes components accompanied by the second and higher order Stokes components have been observed[5]; these anti-Stokes components are believed to occur only as a result of optical frequency mixing.

The stimulated Brillouin scattering in gaseous oxygen and in gaseous argon has not been extensively studied. No experimental data on argon gas have been made available, except a brief note of observation stated by Hagenlocker and his co-workers[6]. An isolated experimental point on SBS in oxygen has been reported by Mash et al[4]. However, no systematic observation of the effect in oxygen was undertaken before the present investigation. It has been demonstrated by some workers[7] that SBS in pure argon gas cannot be produced easily at gas pressures lower than 2000 psi using moderate input laser powers up to 30 MW.

Stimulated Thermal Rayleigh Scattering (STRS)

Although most types of spontaneous light scattering have found their counter parts in stimulated light scattering immediately after the giant-pulse laser was invented, for the central "sharp" Rayleigh peak in Brillouin-Rayleigh triplet no corresponding stimulated process had been observed for some time. Following the theoretical prediction by Herman and Gray[8], STRS was first observed in liquids by Rank, Cho, Foltz and Wiggins[9], and in gases by Wiggins, Cho, Dietz and Foltz[10]. As discussed above, spontaneous Rayleigh scattering is associated with non-propagated thermal fluctuations which influence the density in the medium to produce light scattering. In order to find a stimulated process corresponding to this scattering, laser light absorbing molecules capable of accentuating thermal fluctuations were introduced into the medium. For STRS in gases, the authors have used NO_2 and I_2 molecules as absorbers in compressed gas mixtures of CO_2-NO_2, N_2-NO_2, and N_2-I_2. The scattered light in STRS shows an up-shift (anti-Stokes shift) in its frequency from the laser frequency, the magnitude of which is approximately one-half of the half-intensity width of the incident laser radiation as predicted by the theory. The threshold power for STRS in the gas mixtures has been experimentally investigated by Dietz[11] and found to follow the theoretical conclusion of Gray and Herman[12] reasonably well. As will be shown below, the threshold power as a function of the gas density is largely dictated by the thermal diffusion property of the gas mixtures.

Resumé of Gray-Herman Theory[12] on STRS

The theoretical treatment of the process of STRS was carried out by solving a set of coupled linearized hydrodynamic equations for the gas laser field interaction in a steady state regime. The main equations to couple the electromagnetic field and the material medium is given by,

$$\frac{\partial^2}{\partial t^2}\rho(t) - \frac{c_0^2}{\gamma}\nabla^2\rho(t) - \frac{n}{\rho_0}\nabla^2\frac{\partial}{\partial t}\rho(t) - \frac{c_0^2\beta\rho_0}{\gamma}\nabla^2 T(t)$$

$$= -\frac{n^2-1}{8\pi}\nabla^2 E^2(t) \quad , \tag{1-3}$$

which is the Navier-Stokes equation with a source term, and

$$\rho_0 C_v \frac{\partial}{\partial t} T(t) - \lambda\nabla^2 T(t) - \frac{C_v(\gamma-1)}{\beta}\frac{\partial}{\partial t}\rho(t) = u(t)/\tau \quad , \tag{1-4}$$

which is the head conduction equation. These two equations have to be coupled with the diffusion equation for stored internal energy density u,

$$\frac{\partial u(t)}{\partial t} - D\nabla^2 u(t) = \frac{nc\alpha}{4\pi}E^2(t) - u(t)/\tau \quad , \tag{1-5}$$

in order to take account of effective relaxation time for thermalization of the absorbed energy. The nomenclatures used in the above Eqs. (1-3) - (1-5) are consistent with those in the original paper by Gray and Herman[12]. The following terms are redefined here to clarify the points which are relevant for the present study:

$\rho(t)$ and $T(t)$ are the density fluctuations and temperature fluctuations, respectively. $E(t)$ is the optical electric field which is

the sum of the laser field $E_L(t)$ and the backscattered field $E_s(t)$. α, D, and ρ_0, respectively, are the absorption coefficient, the diffusion constant, and density of the medium.

Using the stationary plane wave approximation for the fluctuations and the fields, the gain function, $G_R(\omega)$ for STRS, has been derived. The authors derived the effective maximum Rayleigh gain, $(G_R^{eff})_{max}$, after taking the finite laser linewidth into consideration as follows:

$$(G_R^{eff})_{max} = \frac{3^{3/2}(n^2-1)}{16\pi n} \frac{n^2+2}{3} k_s |E_L|^2$$

$$x \frac{\beta c\alpha}{\rho_0 c_p} \frac{1}{\{\Gamma_L + \frac{1}{2}(\Gamma_R+\Gamma')\}^2} \frac{1}{\tau} \qquad (1\text{-}6)$$

where $\Gamma' = 2(1/\tau + Dk^2)$; and

$$\Gamma_R = 2\lambda k/\rho_0 c_p \cdot$$

Consequences of the above theory are:

(1) The frequency shift for the maximum gain, ω_{max}, is given by

$$\omega_{max} = - 1/2\sqrt{3} \{\Gamma_L + \tfrac{1}{2}(\Gamma_R + \Gamma')\} \qquad (1\text{-}7)$$

where the spontaneous Rayleigh linewidth, Γ_R $(= 2\lambda k^2/\rho_0 c_p)$, and Γ' are both assumed to be substantially less than the laser linewidth, Γ_L. The negative sign above indicates an anti-Stokes shift.

(2) The threshold input power, P_{th}, follows from the following relationship:

$$\alpha \text{ (power for a given level of scattered light)}$$
$$\propto 1/\rho_0 \, (1 + \rho_n/\rho_0)^2 \qquad (1\text{-}8)$$

with ρ_n, the density at which Γ_L and $\frac{1}{2}(\Gamma_R + \Gamma')$ are equal, lying typically in the range 2 - 3 amagats.

(3) They were able to deduce an expression for α_{cr}, the value of α for which the gain for STRS and that for SBS are equal. Substituting appropriate experimental and other material parameters in the above results, it has been shown that the experimental results obtained agreed reasonably well with the theory.

Statement of the Problem

Stimulated scattering in pure argon has been investigated by Mink and Rado[13], and by Dietz, Cho, Rank and Wiggins[7]. Among other things, they observed from argon the backscattered light containing a frequency component which is anti-Stokes shifted and resembles STRS closely. Although pure argon does not absorb at laser frequency, the authors, Dietz et al, reasoned that the absorbed light may be attributable to STRS if one assumes that the absorption is present in high electron density plasma known to exist in argon.

In the course of investigation of the anti-Stokes shifted light in argon, it was found that a small percentage of impurity in the gas plays an important role for the production. In this thesis, it is intended, therefore, to conduct a systematic experimental investigation for the production of the stimulated light in pure argon as well as in Ar-O_2 mixtures, O_2 being introduced as impurity. It is

also hoped that the results of the present investigation may lead to the possible explanation for the origin of this scattering.

The present work also includes the experimental measurements of SBS in argon and in oxygen. An attempt is made to determine the density dependence of the hypersonic velocities in these gases. All the experiments were carried out at room temperature.

CHAPTER II

EXPERIMENTAL APPARATUS AND PROCEDURE

A. Apparatus

The experimental set-up used in the present investigation is schematically shown in Fig. 1. The detailed account of the set-up will be discussed below. Two Fabry-Perot etalons, each in combination with a camera, were used to record the frequency profile of the back-scattered light from gas samples contained in the high pressure gas cell. A streak camera was used in the later stage of the present experiments to observe the temporal development of the laser induced plasma formed in the gas samples.

(1) Laser System

A Korad K-1500 ruby laser system, modified to operate as a passively Q-switched oscillator by removing the amplifier laser head and the Pockels cell, active Q-switch, was used throughout the present experiment. A Czolchralski "standard" quality ruby rod, doped with 0.05% of Cr_2O_3, was optically pumped by a helical xenon lamp in the optical cavity to produce high intensity laser beams. The rod was of a cylindrical form, 4" long and 9/16" in diameter, the cylindrical axis making an angle of 60^o with respect to the "c"-axis of the crystal. Each end surface of the rod was flat within a tenth of a wavelength at 6943Å, and was anti-reflection coated. The end surfaces were parallel within 2 - 4 seconds of arc. The temperature of the ruby rod was

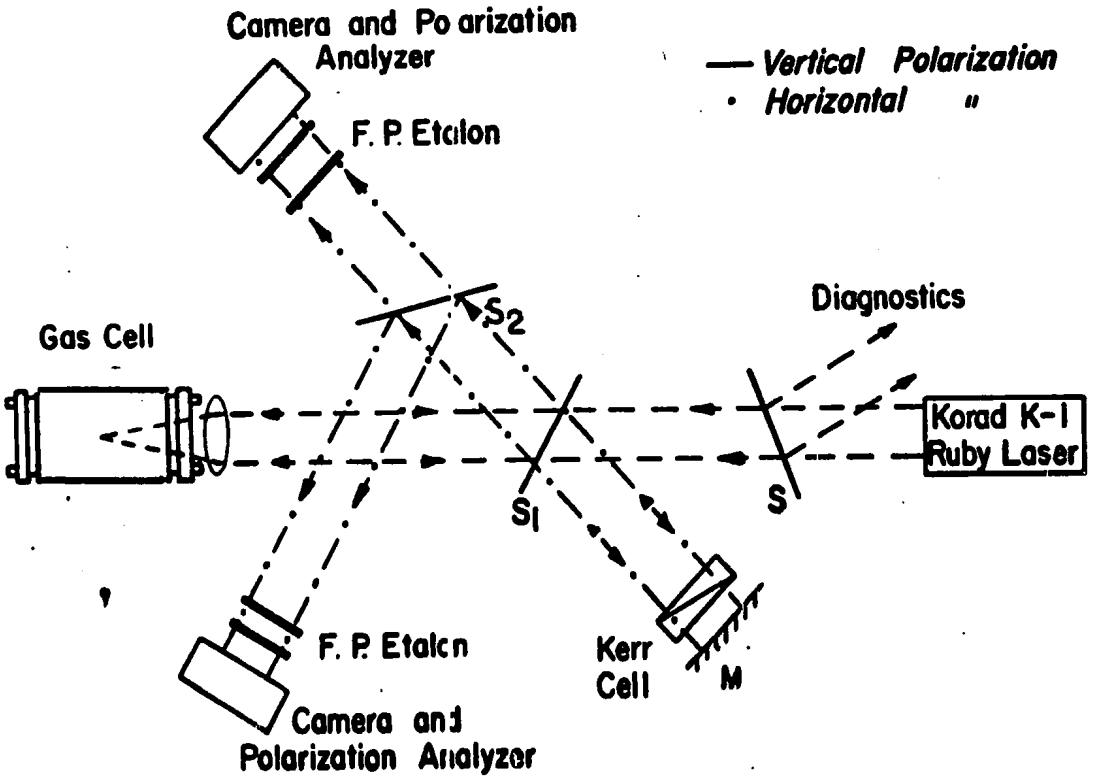

Fig. 1. Optical arrangement.

controlled by continuously circulating water in conjunction with a Lauda-Brinkmann circulator Model K-2/R.

The laser system was passively Q-switched by means of a bleachable dye, cryptocyanine solution in methanol, contained in an open liquid cell. The cell consists of two optically flat fused quartz windows, each 3/8" thick and 1" in diameter, which are cemented on a quartz spacer of 1/8" thick. The spacer has a small opening on its side for filling and adjusting the dye solution. The outside surface of the front window is anti-reflection coated to avoid the reflection loss while the inside surface of the back window is coated for near 100% reflectivity. When the cell was inserted in the laser cavity, the back window served as the rear reflector of the laser cavity. The front reflector of the laser cavity is an optically flat sapphire plate, with its orientation in such a way that laser output would be linearly polarized. The orientation of the ruby rod is adjusted so that the "c" plane of the ruby rod is horizontal, thus ensuring that the plane of polarization of laser light will be vertical. In order to produce the laser beam of a single pulse and of a single longitudinal cavity mode, the optical alignment of the laser cavity and the concentration of the dye solution were carefully adjusted.

The total laser energy of each pulse was measured with a TRG Model 100 Thermopile which was connected to a Keithley 150B Microvoltmeter. This detection unit, a part of the "diagnostics" which is shown in Fig. 1, detects the sampling beam reflected off a beamsplitter placed immediately adjacent to the output side of the laser cavity. In order to calibrate the "diagnostics" energy readings, a Korad KJ-3

Calorimeter was used to make a direct energy measurement for the laser pulse which is incident on the gas cell. As a second part of the diagnostics, an ITT F-4000 photodiode with S-1 spectral response and a 0.5 nanosecond risetime, in conjunction with a Tektronix Model 519 oscilloscope was employed to record the temporal profile of each laser pulse. In the course of the present investigation, it was often necessary to reduce the laser energy incident on the gas cell without undue changes in the pulse width. This was achieved by inserting an attenuating liquid cell containing copper sulphate in water solution and/or a stack of thin glass plates between the laser and the beam-splitter for the diagnostics. The laser energies used in these experiments were in the range of 0.02 to 1.50 joules. The pulse width, more precisely the temporal half-intensity width, of each laser pulse was approximately 20 nanoseconds. Although the spectral half-intensity width of the laser beams fluctuated from one pulse to another, the typical values were in the range of 0.01 to 0.04 cm^{-1}. The beam divergence is 3 - 5 milliradian.

(2) Fabry-Perot Interferometers

The frequency profiles of the laser light as well as the scattered light were studied using Fabry-Perot etalons. Each etalon consists of a pair of parallel fused quartz plates 3.5" in diameter and 3/4" thick, separated by brass spacers with invar inserts. The inside surface of each etalon plate was coated with a zinc sulphide film, with a surface flatness within 1/40 of a wavelength at 6328Å. The reflectivity of the coated surface is 85% at the wavelength 6943Å.

In the present investigation, interferometers of two different spacings, 6.47 cm and 2.24 cm, were used, given the inter-order separations, 0.0773 cm^{-1} and 0.223 cm^{-1}, respectively.

(3) Gas Cells

The gas cell used for most of the experiments for this thesis was of a 10 cm path length, transmission-type high pressure gas cell which was previously described[18]. The cell body, constructed of a stainless steel cylinder, 3.5" in diameter with a bore of 3/4" in diameter, was originally designed to withstand pressures up to 30,000 psi. A modification was made to the entrance window aperture of the cell to accommodate the whole laser beam into the cell without obstruction; the light guide which was originally present inside the central bore was removed to allow the free passage of the light beam. Circular Pyrex glass plates, 15/16" in diameter and 3/16" thick, were cemented onto the window plates with Glyptal Cement to serve as the entrance and exit windows.

Another gas cell of similar design with a side window was used for a brief period to study the dynamics of the laser-induced plasma. The detailed description of this cell is not to be made in the present thesis because only preliminary results on the plasma will be discussed here in relation to other observations.

B. Experimental Procedure

(1) Optical Arrangement

In preparing for the experimental set-up, the following points

were taken into consideration. Firstly, to identify the backscattered anti-Stokes shifted light, it is necessary to adopt the "polarizational separation" method which has been used by other investigators[7]. The method of "polarizational separation" can be used to measure a small frequency difference between two light beams; it is specially useful when the frequency difference is of an order of the breadth of the spectral lines involved. Secondly, possible generation of both SBS and STRS in the gas samples requires simultaneously observations with two interferometers of different spacers. The optical set-up shown schematically in Fig. 1 was thus arranged to accommodate these requirements.

Laser light was focused in the gas cell with a 17.5 cm focal length lens. The backscattered light was collimated by passing through the focusing lens and reflected by a beamsplitter, S_1, in Fig. 1, to pass through the Fabry-Perot etalon and then into a camera. During the course of studying the anti-Stokes shifted light in Ar, the distance between the laser system and the gas cell was kept at a distance of 560 cm to prevent the possible reamplification of the backscattered light by the laser. The beamsplitter, S_1, a Kerr cell containing nitrobenzene, and a mirror served to achieve the first objective above. A fraction of the laser beam reflected from S_1 was first directed through the Kerr cell onto M. The beam reflected by M was then allowed to pass through the Kerr cell for the second time. For operation, the Kerr cell was so oriented that the direction of the D.C. electric field made a 45^{o} angle with respect to that of the polarization of the laser beam. With an applied D.C. voltage of 32 KV, quarter wave retardation

was introduced between the "slow" and "fast" components of the light emerging each time from the Kerr cell. The laser light, having travelled through the Kerr cell twice, entered the etalon with its plane of polarization rotated through a 90^{o} angle. Polarized analyzing sectors were placed directly in the front of the photographic plates inside the camera in order to distinguish the laser light, of which the plane of polarization has been rotated, from the backscattered light having the same polarization as the incident. The polaroid sectors were arranged to form four quadrants, two adjacent sectors analyzing light components of two mutually perpendicular polarizations.

Care was taken to eliminate parasitic light, possibly originating from the stray reflections at various optical surfaces and/or from the imperfect polarizations of the light components. Photographic plates used in the present observations were Kodak type 1-N spectroscopic plates.

(2) High Pressure Gas Sample Preparation

In the experiments, the high pressure gas samples were prepared by means of a cryogenic method using a thermal compressor. For the pure gas samples, care was taken to ensure each sample was free from contamination by other gases. The pure argon gas samples, for which the purity was of paramount importance, were obtained from a cylinder supplied by Matheson of Canada Limited. The total impurity quoted was less than 11 parts per million. For each set of $Ar\text{-}O_2$ mixture experiments, a mixture was first prepared inside the gas cell at a total pressure of approximately 5000 psi. The pressure of the

mixture was then lowered in a number of steps at which the experiments were carried out. In preparing a mixture, oxygen gas from a commercial cylinder was first admitted into the gas cell at a pressure in the range of 15 to 100 psi. Its initial pressure was measured with a mercury manometer for pressures below 30 psi and with a Bourdon tube-type pressure gauge for pressures above that value. Argon gas was then introduced to the cell until the total pressure reached approximately 5000 psi. The final total pressure of Ar-O_2 mixture as well as those of pure argon were measured with a Bourdon tube-type pressure gauge. For each mixture, more than 12 hours were allowed to ensure the uniform mixing of gases.

The gas pressures were converted to densities in amagats using the published isothermal data[14],[15]. The concentration of oxygen in each mixture was obtained by taking the ratio between the partial density of oxygen and the density of the mixture in amagat unit. In order to check the validity of this method, a series of experiments keeping a constant density of oxygen inside the cell and adding argon gas in steps were carried out for consistancy in results. Some of the mixture samples were also analyzed by using a CEC 21-614 Residual Gas Analyzer in the Chemistry Department of this University to ascertain the concentration ratios as determined above. All the experiments were performed at room temperature.

(3) Determination of Frequency Shifts

The frequency difference between the scattered light and the laser light was determined from the measured values of the diameters of

the concentric circular rings produced with the Fabry-Perot interferometer. As two light beams pass through the interferometer, as described in Section A.(2) in this chapter, two sets of fringes are simultaneously photographed. After the individual rings in both sets of fringes are identified in terms of the corresponding orders of interference, the diameters of approximately 12 consecutive rings in each set are measured by means of a Gaetner Comparator. The smallest ring measured is usually the second one from the centre of the fringe patters, for the innermost ring may introduce unwarranted measuring errors to the comparator readings due to its broadness. The measured values of diameters give rise to the "fractional order difference", Δm, by the following equation:

$$\Delta m = \frac{D_m^2 - D_m'^2}{D_m^2 - D_{m-1}^2} \quad , \tag{2-1}$$

where D_m is the diameter of the m^{th} order of the laser spectrum;

D_{m-1}, the diameter of the $(m-1)^{th}$ order of laser spectrum; and

D_m', the diameter of the m^{th} order of the backscattered light spectrum. The frequency shift, ω, in unit of cm^{-1}, is

$$\omega = \Delta m \frac{1}{2s} \quad . \tag{2-2}$$

Here s is an interferometer spacing, and the quantity 1/2s is specified as the interorder separation.

C. Error Estimates

(1) Errors in Frequency Shift Measurements

The mathematical approximation employed in deriving the

equation (2-1) is solely through the following relationship between a given interference fringe diameter D and the corresponding angle θ subtended from the camera lens:

$$D = 2f\theta \quad , \tag{2-3}$$

where f is the focal length of the camera lens. This approximation is good in the order of $(\frac{D}{2f})^2$. In the present case, with $D \lesssim 2$ cm and f = 60 cm, equation (2-1) is accurate to 1 part in 10^4.

The main source of the possible error in the values of the frequency shifts can be attributed to the measurement of the diameters of the interference fringes. As the microscope of the comparator scans across the fringes through the centre of the interferogram, extreme care has to be taken in locating the exact centre. However, the error arising from this is estimated to be much smaller than that arising from the uncertainty in locating the intensity maximum of each interference ring which is estimated to be approximately one-tenth of the linewidth. For the laser line of $0.02\,cm^{-1}$ width, the error is therefore about $\pm$ 0.002 cm^{-1}. This error corresponds to 5% and 20% of the values of SBS and STRS shifts, respectively. The frequency shift obtained from one interferogram is found by taking the algebraic mean of all the values at different interference orders. The standard deviation computed for the mean agreed well with the measurement error estimated above.

(2) Errors in Threshold Power Determination for STRS

For the determination of the threshold powers, there are two

possible sources of error. One is in the power measurements; the other is in detectibility of the spectral components on the photographic plates. The error in power measurement depends on the errors in the measurement of both the energy and the temporal half-width of the laser pulse. The energy measurement introduces an estimated error of 5%, which is concluded by comparing the output readings of two independent calorimeters; this value is confirmed by the manufacturer's quoted value of 5% in measurement error. The rise time of the photodiode is, as quoted by the manufacturer, 0.5 nanoseconds; that of oscilloscope 0.35 nanoseconds and the combined rise time as calculated using an equation given by the manufacturer is 0.6 nanoseconds. In measuring the oscilloscope trace to obtain the temporal half-width of each pulse, the uncertainty arising from the width of the trace line is estimated as ± 1.5 nanoseconds. The total error in the value of the half-width of the temporal profile is about 1.6 nanoseconds which corresponds to 8% for a 20-nanosecond pulse. The total percentage of error in the power value can be estimated as 10%.

For the determination of the threshold power at a given pressure, a series of interferograms were taken at predetermined power increments and they were carefully examined to pick a power at shich STRS was just detectable. The power increment between two consecutive shots was typically from 10% to 30%. Therefore, the maximum uncertainty in selecting the right power from the photographic plate was approximately ± 20%. In taking account of all the factors considered above, the determination of threshold power has an overall error of 22%.

CHAPTER III

RESULTS AND DISCUSSION

A. Stimulated Thermal Rayleigh Scattering (STRS) in Ar and Ar-O_2 Mixtures

Reproductions of typical interferograms of backscattered light in various samples are presented in Figs. 2 and 3. A Fabry-Perot etalon with a free spectral range of 0.0773 cm^{-1} was used for both sets of interferograms. The results shown in Fig. 2 were chosen to illustrate the effect of O_2 concentration on the backscattered light in Ar-O_2 mixtures. For all the gas samples presented in the figure, the density of 98 amagats and the input laser power of 4 MW were kept constant. The quadrant of each interferogram shows the Febry-Perot fringes of laser light. Fig. 3 shows that the backscattered light in pure argon is slightly anti-Stokes shifted from the incident laser frequency, and its intensity gradually decreases and eventually disappears as the oxygen concentration is increased. It is also noted that this strong back-scattered light shows the gain narrowing characteristic of the stimulated scattering. In Fig. 3, a set of interferograms similar to those in Fig. 2, but at a higher density of 339 amagats, are shown. Input laser powers for these samples are kept as closely as possible to a constant value of 6.0 MW. While the general features of the anti-Stokes shifted components are similar to those observed at lower densities, in addition, the stimulated Brillouin components are now observed in the gas mixtures of a certain concentration range. At this density and input power, both the stimulated thermal Rayleigh and the

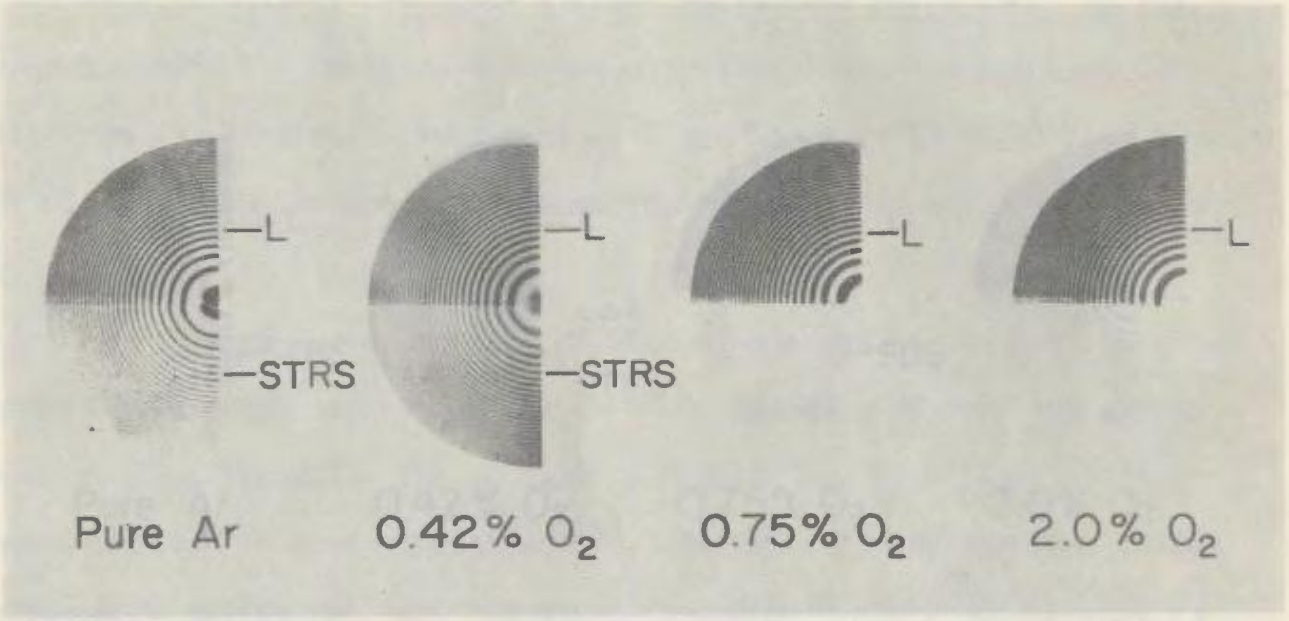

Fig. 2. Interferograms of the backscattered light in pure Ar and in three Ar-O_2 mixtures with laser input power of approximately 4 MW. An etalon spacer of 6.47 cm thick is used. Total density of each sample is approximately equal to 98 amagats.

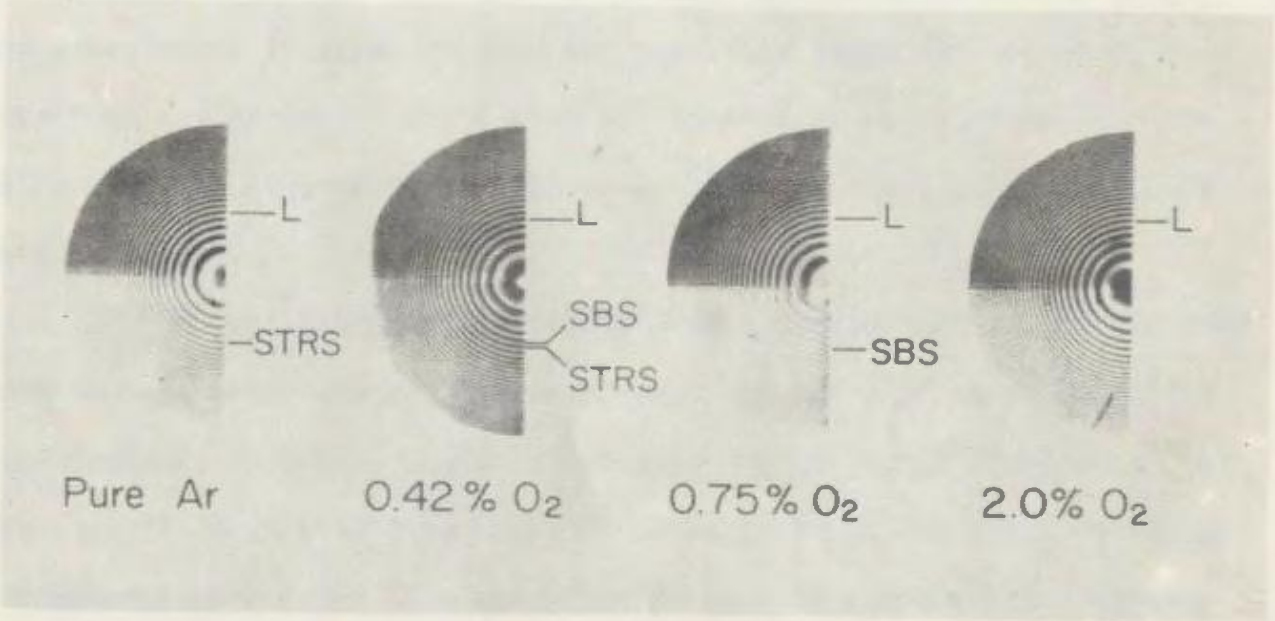

Fig. 3. Interferograms of the backscattered light in pure Ar and in three Ar-O_2 mixtures with laser input power of approximately 6 MW. An etalon spacer of 6.47 cm thick is used. Total density of each sample is approximately equal at 339 amagats.

stimulated Brillouin components are absent in the mixtures containing oxygen concentration more than 2%. It is noted, however, that in the last interferogram of Fig. 3 the backscattered light seems to consist of the unshifted laser frequency without noticeable narrowing. It has been experimentally verified that the unshifted light did not seem to arise from any parasitic light such as laser light reflections from the cell windows or other optical components, and imperfect polarization of the laser light.

The anti-Stokes shifted component observed in the backscattered light in pure argon gas as well as in Ar-O_2 mixtures of very low oxygen concentrations resembles the stimulated thermal Rayleigh light which has been identified in absorbing gases[10]. In Table I, the measured values of frequency shifts for this component in various samples under varying experimental conditions are given. The magnitude and the direction of this frequency shift agree well with the nature of the stimulated thermal Rayleigh scattering (STRS) experimentally observed. The gas samples in the present study, however, do not exhibit any measurable absorption at the ruby laser frequency, 6943Å, if a light of conventional intensity is used. Since this absorption of laser energy is essential for the production of STRS, it is difficult to identify this scattering in argon with STRS without any further experimental evidence. It is noted, however, that while the frequency shifts are in general agreement with STRS shifts in their orders of magnitude, the variation of the shifts with various parameters involved in the present study seem negligible within the experimental error. It is especially significant

TABLE I. Observed anti-Stokes shifts for the backscattered light from argon and from argon-oxygen mixtures. Pertinent experimental data including the half-intensity width are also given.

O_2 concentration (%)	Total density (amagats)	Input laser power (MW)	Half-intensity laser linewidth (cm^{-1})	Measured anti-Stokes shift (cm^{-1})
—	55	4.8	.013 ± .002	.011 ± .001
—	237	2.0	.014 ± .001	.011 ± .003
—	339	8.5	.026 ± .002	.009 ± .002
—	339	17.0	.028 ± .002	.010 ± .002
.42	98	4.0	.022 ± .002	.009 ± .001
.42	98	30.0	.022 ± .002	.015 ± .002
.42	163	13.0	.018 ± .002	.012 ± .002
.42	200	9.0	.026 ± .004	.013 ± .004
.75	98	7.8	.016 ± .002	.007 ± .002
.75	200	9.5	.020 ± .002	.013 ± .003
.75	200	10.5	.025 ± .002	.011 ± .002
2.0	98	14.0	.018 ± .002	.010 ± .001

that the observed anti-Stokes shift does not seem dependent on the laser line width; such dependence has been observed in STRS in absorbing liquid[9].

The observed values of the threshold input laser power for the anti-Stokes component in pure argon gas and in Ar-O_2 mixtures are presented in Table II. This component is identified as STRS in the table, the justification of this designation is to be given later. Those data are also plotted against the gas density as shown in Fig. 4. It can easily be seen that the threshold power curves for Ar-O_2 mixtures are shifted upward from that for pure argon, and the shifts are quite drastic as compared with their oxygen concentrations. The striking feature of the figure is that, for each Ar-O_2 mixture, there exists a certain critical value of density above which no STRS is observed. This suppression of STRS in the mixtures was not observed in pure argon. All the Ar-O_2 mixtures investigated with more than 2% oxygen concentrations failed to produce the anti-Stokes shifted component.

For the purpose of comparison, exploratory experiments with Ar-He, Ar-H_2 and Ar-N_2 mixtures were also carried out to investigate the anti-Stokes shifted component. The preliminary results obtained in Ar-H_2 and Ar-N_2 mixtures show in general qualitative agreements with the present results in Ar-O_2 mixtures, while those in Ar-He mixtures exhibit entirely different behaviour. The intensity of the anti-Stokes shifted component does not seem to be affected by the presence of He impurity even at the He concentration of as high as 10%.

TABLE II. Observed threshold input laser powers for STRS in pure Ar and Ar-O_2 mixtures.

Pure argon		0.42% O_2		0.75% O_2		2.0% O_2	
Total density (amagats)	P_{th} (MW)	Total density (amagats)	P_{th} (MW)	Total density (amagats)	P_{th} (MW)	Total density (amagats)	P_{th} (MW)
339	1.27	238	2.87	193	3.52	98	5.55
306	1.66	200	2.22	178	3.70	84	6.25
273	1.71	164	2.53	151	3.78	75	7.6
238	1.41	132	3.32	130	4.54	69	8.10
200	1.85	98	2.96	98	5.25	59	8.85
164	2.02	65	4.79	65	7.70	38	21.1
98	2.64	51	6.80	51	9.02		
65	3.85			38	15.2		
51	4.45						
38	6.25						

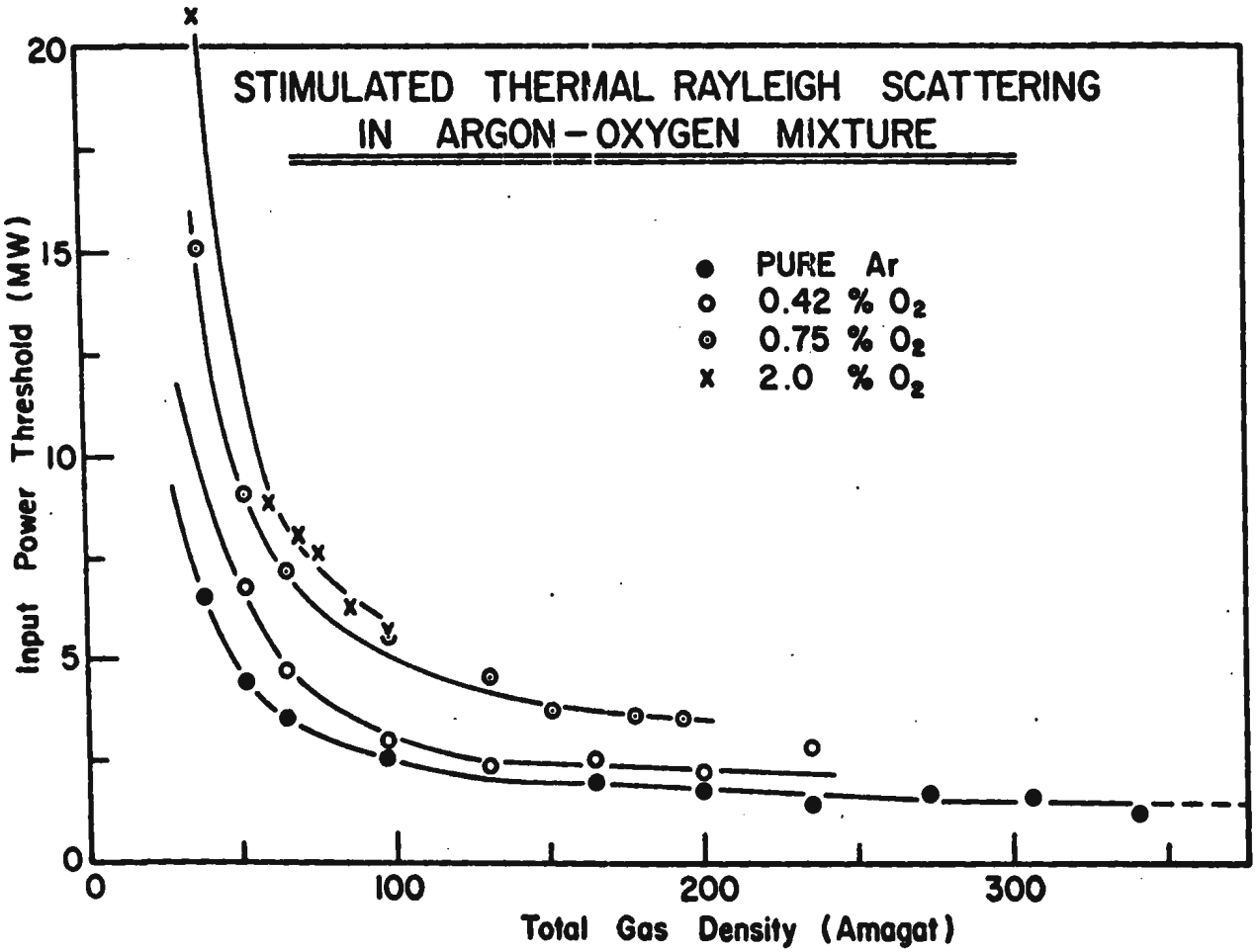

Fig. 4. Plots of input threshold power versus total gas density from stimulated thermal Rayleigh scattering in pure Ar and in Ar-O_2 mixtures.

B. Discussion of STRS and the Modification to the Gray-Herman Theory

As has been assumed in the preceding sections, the anti-Stokes shifted components observed in the backscattered light can be interpreted to arise from the stimulated thermal Rayleigh scattering in argon. Argon atoms in the ground state are not known to have an appreciable absorption coefficient at the ruby laser wave length, 6943Å, under the normal experimental conditions. With the formation of laser induced plasma, however, argon ions and highly excited neutral argon atoms present in the plasma may initiate the thermalization process which is essential for STRS. Although the radiative relaxation times for a number of excited states of argon atoms and of argon ions have been reported to be in the order of 10^{-8} sec, there are several known metastable states[16] for which the radiative relaxation times are on the order of 10^{-5} sec. Argon atoms in these metastable states may effectively contribute to the thermalization process. Since the energies of the known metastable states are greater than 10 ev above the ground state, excitation of argon atoms to the metastable states can only take place either by a direct multiphoton process or in the laser induced plasma. If the latter mainly contributes to the excitation mechanism, it is reasonable to assume that the laser induced absorption coefficient which arises from the excited neutral atoms and ions is proportional to the laser power since the rate of development of cascade in a given plasma is proportional to the incident laser intensity[17]. Using the value of α assumed here, it can be possible to modify the theory originally proposed by Gray and Herman[12] to describe the present experimental results.

The above conclusion is further supported by the experimental evidence in the Ar-O_2 mixtures. Although the concentration of O_2 in each Ar-O_2 mixture is very small, a rough estimate suggests that the number of O_2 molecules and their derivatives (molecular oxygen, ions and atoms, etc.) present in the plasma is comparable to the number of argon ions and excited argon atoms. It may also be assumed that the cross section for the energy transfer between the excited argon atoms and/or ions and oxygen molecules is much greater than that for thermalization through collisions among these argon partners. Consequently, the effective absorption coefficient of Ar may decrease by the addition of oxygen molecules in the plasma; the STRS can thus be inhibited in the gas mixtures.

In order to discuss the above results theoretically, the Gray-Herman theory for the stimulated thermal Rayleigh scattering process as discussed in Chapter I is modified as follows:

(a) For the scattering in pure argon, the absorption coefficient, α, in Eq. (1-5) is replaced by $\tilde{\alpha}|E_L|^2$. Here, $\tilde{\alpha}$ is a proportionality constant having proper dimensions, and E_L is the amplitude of the laser field. It is implicitly assumed that $\tilde{\alpha}$ is independent of the gas density. The validity of the assumption is not claimed for any value of laser power as well as that of gas density, but the assumption seems reasonable for the laser powers in the neighbourhood of the threshold.

(b) When the oxygen impurity is present, the diffusion constant for the internal energy, D, in Eq. (1-5), can be replaced by $D_0 + D_1$, where D_0 and D_1 are proportional to the densities of argon

and oxygen, respectively. The thermal relaxation time in Eqs. (1-4) and (1-5) are also replaced by τ_m, the thermal relaxation time in the gas mixtures. The resulting set of the modified equations are given as follows:

$$\frac{\partial^2 \rho(t)}{\partial t^2} - \frac{c_0^2}{\gamma} \nabla^2 \rho(t) - \frac{\eta}{\rho_0} \nabla^2 \frac{\partial}{\partial t} \rho(t) - \frac{c_0^2 \beta \rho_0}{\gamma} \nabla^2 T(t) = - \frac{n^2-1}{8\pi} \nabla^2 E(t)^2 \quad , \tag{3-1}$$

$$\rho_0 C_v \frac{\partial}{\partial t} T(t) - \lambda \nabla^2 T(t) - \frac{C_v(\gamma-1)}{\beta} \frac{\partial}{\partial t} \rho(t) = \frac{u(t)}{\tau_m} \quad , \tag{3-2}$$

and

$$\frac{\partial u(t)}{\partial t} - (D_0 + D_1) \nabla^2 u(t) = \frac{nc\alpha E^2(t)}{4\pi} - \frac{u(t)}{\tau_m} \quad , \tag{3-3}$$

By employing the stationary plane wave approximation, one can obtain the following relationship for τ_m in Eqs. (3-2) and (3-3):

$$\frac{1}{\tau_m} = \frac{1}{\tau_0} - D_1 k^2 \tag{3-4}$$

where τ_0 is the thermal relaxation time in pure argon, and k is the magnitude of the vector difference between wave vectors for the back-scattered and incident laser radiation, or

$$k = k_L + k_S \quad . \tag{3-5}$$

Following the above modification to the theory, the maximum effective thermal Rayleigh gain for the STRS in argon are derived for pure argon as well as for Ar-O_2 mixtures. The gain is given by

$$(G_R^{eff})_{max} = \frac{3\sqrt{3}(n^2-1)}{16\pi n} \frac{n^2+2}{2} k_S |E_L|^4 \frac{\beta c \tilde{\alpha}}{\rho_0 c_p}$$

$$\times \frac{1}{[\Gamma_L + \frac{1}{2}(\Gamma_R+\Gamma')]^2} \frac{1}{\tau_0} (1 - \tau_0 D_1 k^2) \qquad (3\text{-}6)$$

where $\frac{\Gamma'}{2} (\equiv \frac{1}{\tau_0} + D_0 k^2)$ is the combined rate for decay of internal energy fluctuations and Γ_R $(= 2\lambda k^2/\rho_0 c_p)$ is the line width associated with spontaneous Rayleigh scattering. As τ_0, Γ_R, and Γ' all vary as ρ_0^{-1}, the product, $D_1\tau_0$, varies as the concentration of oxygen, r, and the remaining is roughly independent of density. The threshold power, P_{th}, is related to the total gas density through the relation

$$P_{th} \propto \frac{1}{\sqrt{\rho_0}} (1 + \frac{\rho_n}{\rho_0}) / \sqrt{1 - Br} \qquad (3\text{-}7)$$

where ρ_n is the density at which Γ' and $\frac{1}{2}(\Gamma_R+\Gamma')$ are equal, since both Γ_R and Γ' are inversely proportional to ρ_0, and B is a dimensionless proportional constant.

(1) For pure argon:

By setting oxygen concentration r to be zero, one obtains immediately the relationship between the STRS threshold power, P_{th}, for pure argon and the argon density, ρ_0, as follows:

$$^0P_{th} \propto \frac{1}{\sqrt{\rho_0}} (1 + \frac{\rho_n}{\rho_0}) \quad . \qquad (3\text{-}8)$$

The functional dependence of the observed threshold powers for STRS in pure argon on ρ_0 is examined by plotting $\sqrt{\rho_0}\ ^0P_{th}$ versus ρ_0^{-1} in Fig. 5. It can be seen that the experimental points lie reasonably well on a straight line, thus confirming the theoretical relationship given in

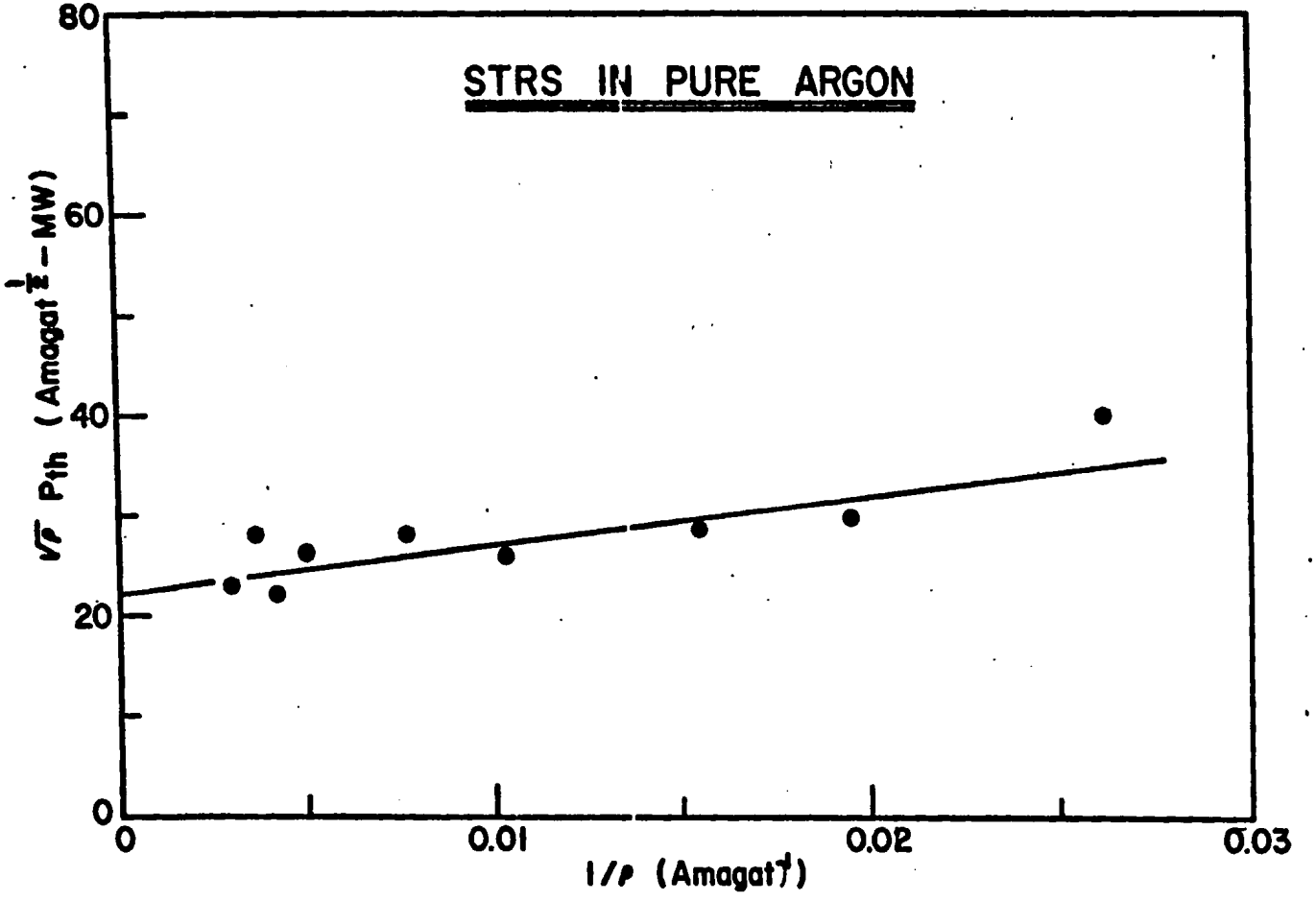

Fig. 5. Dependence of input threshold power for the stimulated thermal Rayleigh scattering in argon on gas density.

Eq. (3-8). The value of ρ_n = 27.3 amagat is found experimentally.

(2) For Ar-O_2 mixtures:

By comparing Eqs. (3-7) and (3-8), the ratio of the threshold powers for the mixtures and that for pure argon at a given total gas density may be obtained as follows:

$$\frac{{}^{O}P_{th}{}^{2}}{P_{th}{}^{2}} = (1 - Br) \quad . \tag{3-9}$$

The experimental values for B are given in Table III for all the mixtures studied. The agreement between B values seems reasonably good within the present experimental error.

Although the above discussion can account for the main feature of the threshold curves in various mixtures, the abrupt termination of an otherwise smooth threshold curve at a certain value of density for each Ar-O_2 mixture, as shown in Fig. 4, is going to be discussed. As one compares the threshold power at each terminal point with the partial density of oxygen determined from the corresponding total density of the gas sample, one finds the striking feature in this ratio as shown in Table IV. The last column of the table shows the ratio between the threshold power and the partial density of oxygen for various Ar-O_2 mixtures. This result seems to suggest that STRS in argon has an additional feature: Although the presence of oxygen impurity in argon can be accounted for by the modified and the decreased gain in the STRS process as considered above, there is a critical limit of input power per oxygen molecule, below which the nonlinear gain for STRS cannot be

TABLE III. Check for the theoretical relationship between the ratio of threshold input powers and oxygen concentration in Ar-O_2 mixtures.

Oxygen concentration r(%)	$^{O}P^2_{th}/P^2_{th} = 1 - Br$	
	$^{O}P^2_{th}/P^2_{th}$	B
0.42	0.56 ± 0.12	1.1
0.75	0.25 ± 0.03	1.0
2.0	0.15 ± 0.03	0.43
		Average 0.8 ± 0.3

TABLE IV. Data related to termination points of "threshold curves" for STRS in argon-oxygen mixtures.

Oxygen concentration (%)	P_{th} at the terminal points (MW)	Total density at terminal points (amagats)	Partial density of oxygen (ρ_{O_2}) (amagats)	P_{th}/ρ_{O_2} (MW/amagats)
0.42	2.9	238	1.0	2.9
0.75	3.5	193	1.4	2.5
2.0	5.6	98	2.0	2.8
				Average 2.7 ± 0.2

large enough to commence the process. This remarkably constant value of the ratio between the threshold power and the partial density of oxygen at terminal points of the threshold curves (Fig. 4) should then represent the average amount of energy required for each oxygen molecule before the thermalization time of excited argon atoms becomes small enough to commence the STRS process in the medium. A rough estimation yields the value of 1.2 ev/O_2 molecule for this critical value. It is interesting to note here that the laser induced plasma in argon does not seem to affect directly the mechanism of STRS, except by creating argon atoms which are capable of thermalization.

As discussed in the above sections, the agreement between the experimental results and the modified STRS theory is reasonably good. More conclusive evidence as to whether the laser induced plasma and its dynamics play a direct role for the production of the STRS component in the backscattered light can only be obtained by systematic investigation of the plasma characteristics in relation with STRS in argon gas. It is further hoped that the present investigation be extended for argon gas with other known impurities, such as other diatomic gases, SF_6, other polar gases, etc., in order to ascertain the validity of the present findings.

C. Stimulated Brillouin Scattering (SBS) in Argon and Oxygen Gases

(1) SBS in argon gas

The stimulated Brillouin scattering in argon gas was studied at densities in the range of 117 to 340 amagats at room temperature.

For calculation of hypersonic velocities with Eq. (1-2), the values of index of refraction of argon for various densities, temperatures and light frequencies had to be estimated from available experimental data[14],[23]. In Table V, the observed Brillouin shifts and the corresponding hypersonic velocities calculated are presented. Sometimes, especially in gas samples at high densities and with high input powers, the second order as well as the first order Stokes component were obtained in SBS interferograms. The frequency difference between the first and the second was assumed to be equal to the regular Brillouin shift, which was used to obtain a second set of hypersonic data presented in the last three columns of Table V. The observed hypersonic velocity in argon is plotted against gas density as shown in Fig. VI. For the purpose of comparison, a representative set of points observed by Lallemand and Longequeue[19] in his spontaneous Brillouin scattering experiments is also presented. In Fig. 6, the solid line represents the data from an ultrasonic measurement of Lacam and Noury[20] at two frequencies, 0.6 and 0.9 MH_z. It is noteworthy that the hypersonic velocities obtained from the second Brillouin components seem to agree well with those from the first components. In general, agreement between the ultrasonic data and the present data seems reasonably good, although there is considerable scatter beyond the estimated experimental error. This scatter of experimental points may be attributable to the power dependence of the frequency shifts in SBS as observed by Mash et al[21], and to the unresolved multimode structure of the laser beam as discussed by Saito et al[22]. They will be discussed in the case of SBS in oxygen in (2) of this section. Dispersion of acoustic waves in compressed argon

TABLE V. Observed SBS frequency shift in argon gas at a given density is given with corresponding values of hypersonic frequency and velocity computed from the shift.

	First Brillouin component			Second Brillouin component		
Density (amagats)	ω_B (cm^{-1})	Hypersonic frequency (GH_z)	C_0 (m/sec)	ω_B (cm^{-1})	Hypersonic frequency (GH_z)	C_0 (m/sec)
117	0.0322	0.966	325			
131	0.0310	0.930	311			
144	0.0324	0.972	325			
158	0.0292	0.876	292			
158	0.0320	0.960	319			
164	0.0365	1.10	364			
164	0.0354	1.06	353			
164	0.0352	1.06	351			
171	0.0318	0.954	316			
186	0.0405	1.22	403			
201	0.0432	1.30	427	0.0406	1.22	410
216	0.0410	1.23	404	0.0432	1.30	425
239	0.0384	1.15	377	0.0453	1.36	444
243	0.0458	1.37	448	0.0434	1.30	425
257	0.0413	1.24	402			
272	0.0270	0.810	262			
272	0.0250	0.750	243			
272	0.0438	1.31	425	0.0447	1.34	434
285	0.0411	1.23	399	0.0426	1.28	413
299	0.0420	1.26	650	0.0465	1.40	449
306	0.0408	1.22	393			
306	0.0406	1.22	391			
306	0.0428	1.28	412			
313	0.0354	1.06	340			
327	0.0390	1.17	374	0.0444	1.33	426
340	0.0428	1.28	409	0.0517	1.55	493

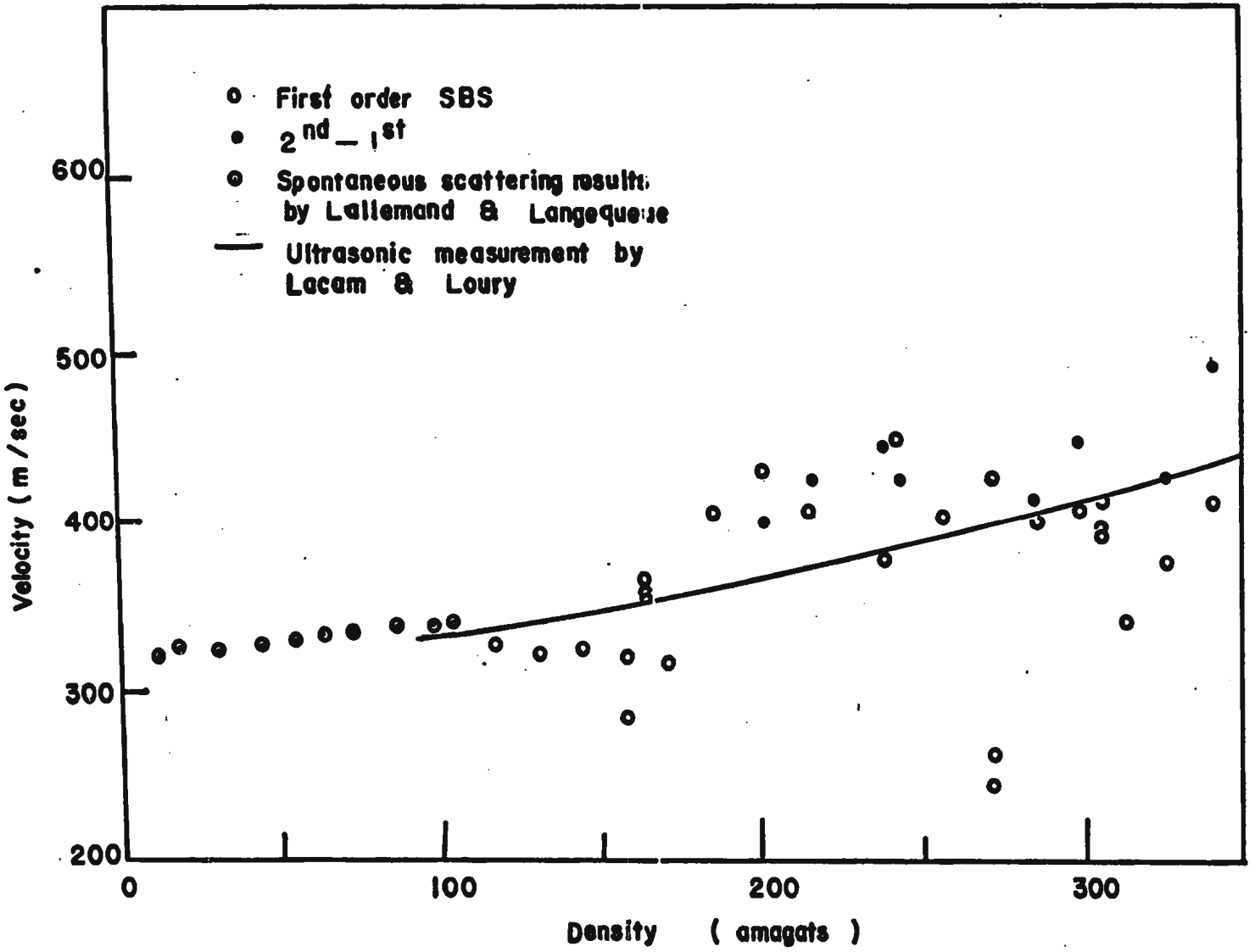

Fig. 6. Hypersonic velocity in gaseous argon as determined from SBS frequency shifts as a function of argon density. Spontaneous scattering data obtained by Lallemand and Langequeue[19], and ultrasonic data by Lacam and Loury[20] are also shown for comparison.

in changing from the ultrasonic frequency to the hypersonic frequency of approximately 1 GH_z in the present density range is shown to be negligible. No appreciable difference in hypersonic velocities in the dilute Ar-O_2 mixture was observed in the present investigation.

(2) SBS in oxygen gas

In Table VI, the measured frequency shifts of the Brillouin components in gaseous oxygen and the corresponding hypersonic frequencies and velocities are presented. Frequently, interferograms for back-scattered light in oxygen showed higher order Brillouin components, quite often as many as four Stokes shifted components. Assuming that the frequency difference between two consecutive components is equal to the corresponding Brillouin shift, the hypersonic velocities are computed and presented in Table VII. The values of index of refraction of oxygen used in the calculations were obtained from the published data[15],[23]. A plot of hypersonic velocities versus gas density using the data in Table VI is shown in Fig. 7. Other experimental data which have previously been obtained from SBS measurements by Mash et al[4], and from spontaneous Brillouin scattering measurement by Lallemand and Longequeue[19] are also plotted in the figure for the purpose of comparison. It is noted that the experimental points fluctuate considerably more than the scatter which may be expected from the estimated experimental error. The uncertainty in the values of the hypersonic speed is estimated to be approximately ± 30m/sec. In fact, the scatter of the value in Fig. 7 is so bad that no definite conclusion may be drawn as to how the speed depends on the density. Reports of

TABLE VI. Observed SBS frequency shift in oxygen gas from first order Brillouin component at a given density. Corresponding values of hypersonic frequency and velocity computed from the shift are also given.

Density (amagats)	ω_B (cm^{-1})	Hypersonic frequency (GH_z)	C_0 (m/sec)	Density (amagats)	ω_B (cm^{-1})	Hypersonic frequency (GH_z)	C_0 (m/sec)	Density (amagats)	ω_B (cm^{-1})	Hypersonic frequency (GH_z)	C_0 (m/sec)
51	0.0275	0.825	283	179	0.0349	1.05	348	266	0.0383	1.15	371
58	0.0270	0.810	277	195	0.0353	1.06	350	266	0.0371	1.11	360
68	0.0306	0.918	323	199	0.0588	1.76	585	266	0.0390	1.17	382
79	0.0260	0.780	265	201	0.0131	0.693	229	273	0.0727	2.18	708
88	0.0317	0.950	323	208	0.0356	1.07	353	273	0.0637	1.91	616
98	0.0344	1.03	349	208	0.0197	0.591	194	274	0.0643	1.93	629
109	0.0308	0.924	312	208	0.0344	1.03	340	278	0.0669	2.01	648
112	0.0360	1.08	364	208	0.0340	1.02	336	281	0.0488	1.46	472
119	0.0368	1.10	372	211	0.0634	1.90	629	281	0.0409	1.23	396
120	0.0323	0.969	326	214	0.0392	1.18	387	281	0.0630	1.89	608
127	0.0431	1.29	635	219	0.0409	1.13	403				
130	0.0324	0.972	326	220	0.0370	1.11	365				
134	0.0445	1.34	448	225	0.0384	1.15	377				
141	0.0351	1.05	353	231	0.0401	1.20	393				
143	0.0445	1.34	448	233	0.0346	1.04	339				
148	0.0510	1.53	511	251	0.0652	1.96	636				
153	0.0454	1.36	455	252	0.0398	1.19	380				
156	0.0346	1.04	347	257	0.0375	1.13	360				
159	0.0465	1.40	465	257	0.0750	2.25	731				
165	0.0484	1.45	483	261	0.0558	1.67	543				
166	0.0437	1.31	436	262	0.0377	1.13	368				
170	0.0616	1.85	611	265	0.0426	1.28	414				
173	0.0563	1.69	561	265	0.0680	2.04	661				
174	0.0461	1.38	460	265	0.0670	2.01	653				

TABLE VII. Observed SBS frequency shift in oxygen gas from the second and higher orders Brillouin components at a given density. Corresponding values of hypersonic frequency and velocity computed from the shift are also given.

Density (amagats)	2nd-1st			3rd-2nd			4th-3rd		
	ω_B (cm^{-1})	Sound frequency (GH_z)	C_0 (m/sec)	ω_B (cm^{-1})	Sound frequency (GH_z)	C_0 (m/sec)	ω_B (cm^{-1})	Sound frequency (GH_z)	C_0 (m/sec)
68	0.0297	0.0891	304						
79	0.0301	0.903	307						
88	0.0309	0.927	314	0.0310	0.930	322			
98	0.0319	0.957	324	0.0325	0.975	330			
109	0.0327	0.981	331	0.0321	0.963	325			
120	0.0319	0.957	322	0.0335	1.01	338			
130	0.0336	1.01	339	0.0348	1.04	351			
141	0.0340	1.02	342	0.0358	1.07	360			
156	0.0349	1.04	350	0.0355	1.07	356			
208	0.0404	1.21	399	0.0375	1.13	371			
220	0.0396	1.19	391	0.0391	1.17	385	0.0367	1.10	362
230	0.0391	1.17	384	0.0290	1.17	383			
240	0.0390	1.17	328	0.0381	1.43	373	0.0391	1.17	383
251	0.0401	1.21	391	0.0396	1.19	386	0.0402	1.21	396
257	0.0421	1.26	409						
261	0.0439	1.32	427	0.0448	1.46	436	0.0379	1.14	396
265	0.0400	1.20	389						
265	0.0439	1.32	427						
271	0.0430	1.29	417	0.0422	1.27	409	0.0413	1.25	404
273	0.0408	1.22	401						
273	0.0466	1.40	458						
278	0.0463	1.39	456						
281	0.0428	1.28	414	0.419	1.26	405	0.0418	1.25	404
281	0.0487	1.46	471						

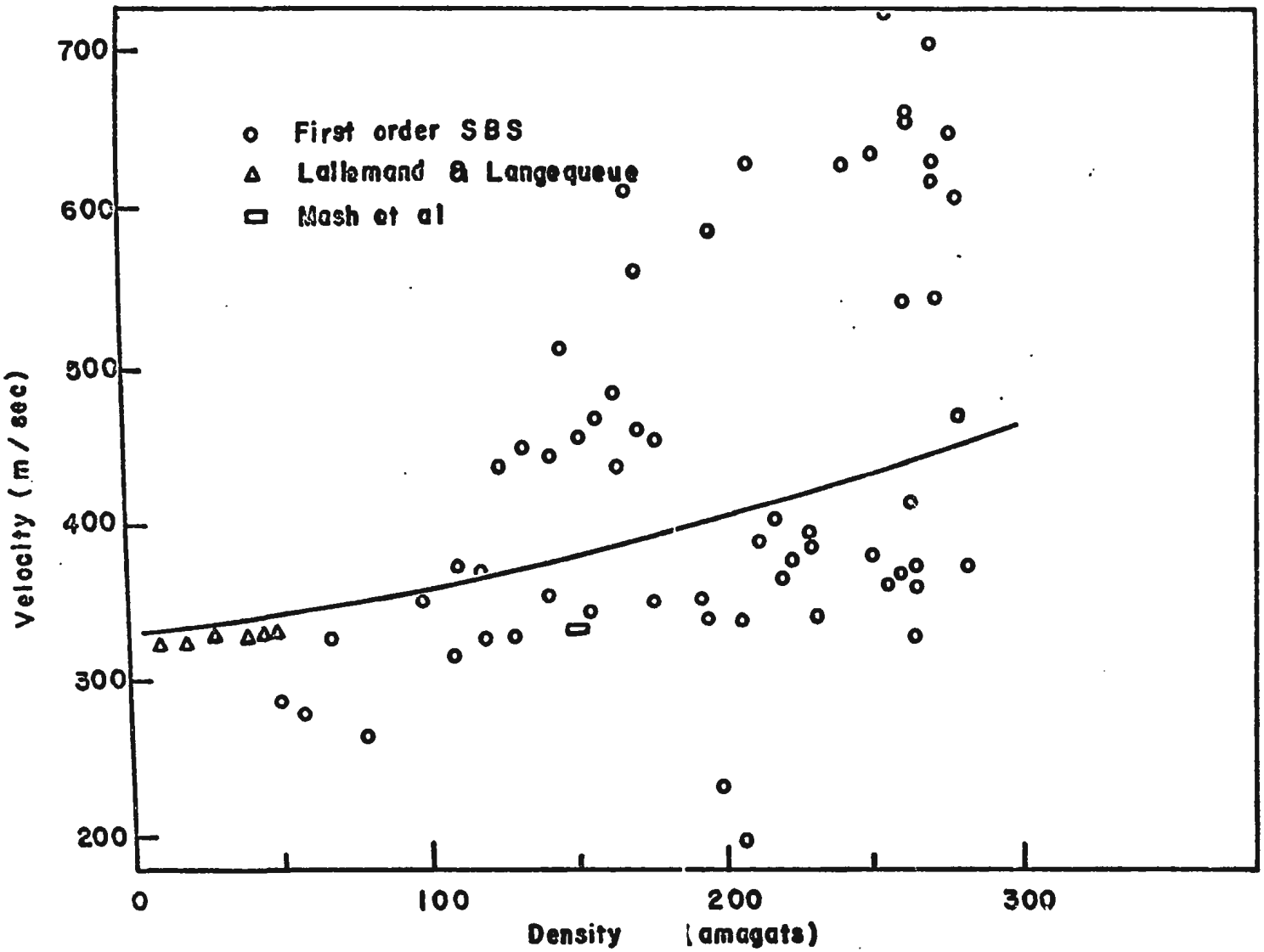

Fig. 7. Hypersonic velocity in gaseous oxygen as determined from 1st order SBS shifts as a function of oxygen density. The solid line represents the calculated values using P-V-T data[29], spontaneous scattering data of Lallemand and Longequeue[19], and SBS measurement of Mash et al[21] are also shown.

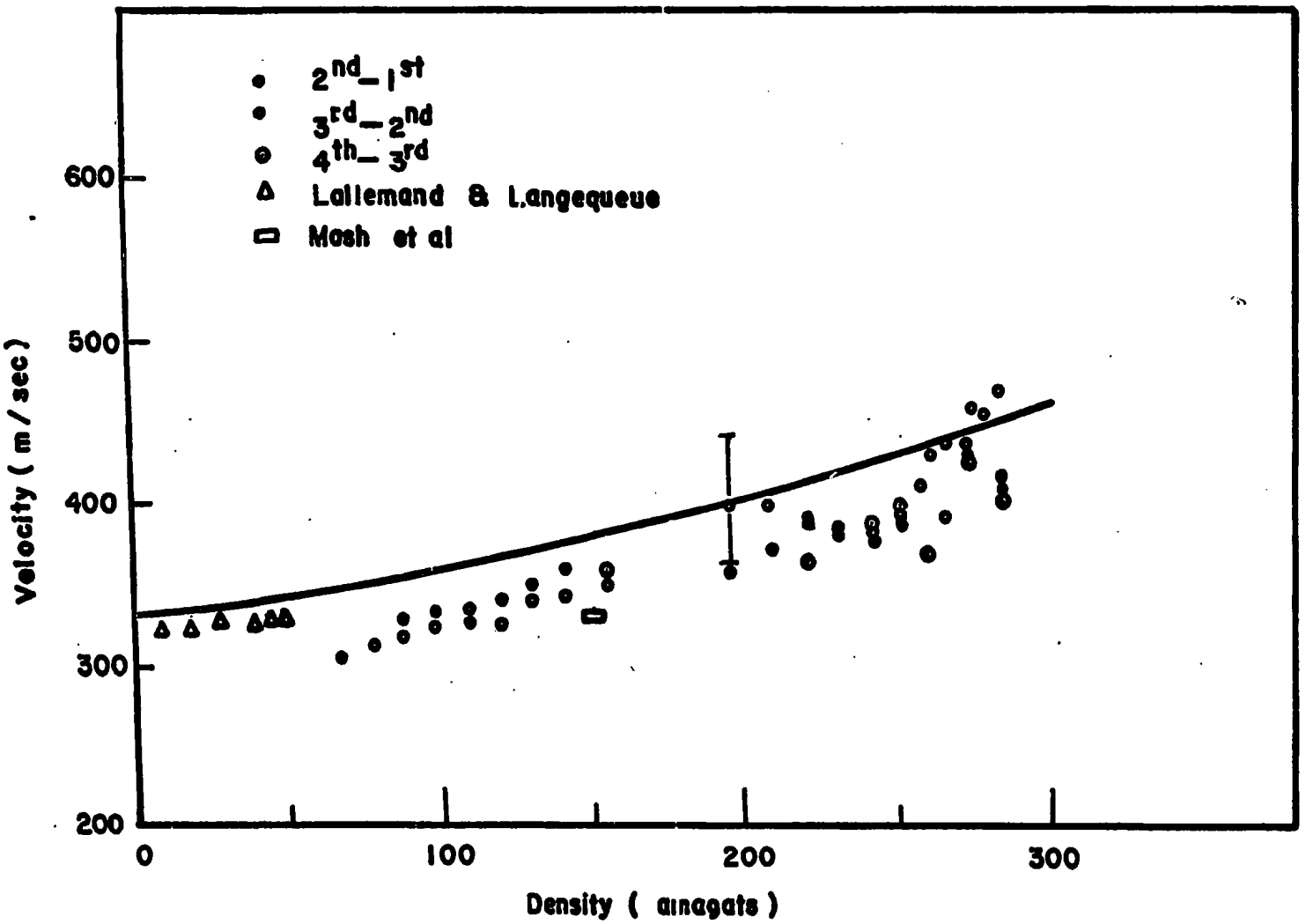

Fig. 8. Hypersonic velocity in gaseous oxygen as determined from higher order SBS frequency shifts as a function of oxygen density. The solid line and previous data are the same as those in Fig. 7. A representative error bar which applied to all experimental points is also shown.

similar difficulties have been made by some authors for the SBS studies in other gases. Nevertheless, their results do not appear to be so bad as the above results in oxygen. As a corresponding plot was made using the hypersonic velocities obtained from the higher order Brillouin components, however, the fluctuation of experimental values showed a surprising improvement. The plot is reproduced in Fig. 8. The solid lines in Figs. 7 and 8 are drawn from the calculated values; the method of calculation is to be discussed in (3) of this section.

In order to explain the large statistical scatter for the hypersonic velocity data obtained in the present work, one has to look closely at the actual production mechanism of SBS in the gas medium. The theoretical consideration of SBS, which has been the subject of many investigators, is usually based on the treatment of the coupling between the strong electromagnetic field and the hypersonic waves in the medium by means of the stationary nonlinear theory. There are, however, a number of competing nonlinear processes which may be present simultaneously with SBS and add to the complexity of the product mechanism of SBS. These include STRS, SRS, the laser induced breakdown and the filament formation in the medium.

After Rank et al[3] noticed the somewhat erratic scatter in the observed hypersonic velocities in N_2, CH_4 and CO_2 at various pressures, Goldblatt and Litovitz[24] explained that this difficulty may be attributable to the multimode structure in the frequency profile of the incident laser light. They thought that SBS might have been produced by a particular mode of laser light which does not necessarily coincide with the central peak position of the total laser profile; this

effect thus introduced the uncertainty in determining the frequency shift of the SBS component from the laser light. Using ruby laser light of very low power (0.5 ∿ 1.0 MW) and very narrow line width (0.003 ∿ 0.006 cm^{-1}), Saito et al[22] recently demonstrated that the scatter of the experimental data obtained in the compressed CO_2, N_2 and CH_4 gases can indeed by practically eliminated. On the other hand, Mash et al[21] showed that the SBS shifts in gases depend also on the intensity of the incident laser light, the shift being smaller with the higher intensity of incident laser light. Recently, Wang[25] showed theoretically that the velocity of sound observed in SBS should be smaller than the adiabatic sound velocity by an amount directly related to the intensity of the laser field. The predicted velocity shifts are sizeable for gases, they remain small for liquids. It is worthwhile to note that Wang's theory is based on the assumption that breakdown does not occur in the gas. The theory fails, however, to explain the agreement between hypersonic velocity measurements in gaseous CH_4 in both spontaneous Brillouin scattering and in SBS as observed by Saito et al.

In the present investigation, the incident laser light with the line width in the range of 0.02 ∿ 0.04 cm^{-1} was used. The power density of the laser beam at the focal region in the gas is estimated as in the range of $5 \times 10^9 \sim 7 \times 10^{10}$ W/cm^2. As can be seen in Fig. 7, the average scatter of points for the first Brillouin component of oxygen exceeds the half width of the laser beam, and predominantly in the direction of the larger frequency shift. It may be concluded, therefore, that the multimode structure of the laser beam is not solely

responsible for this scatter. When careful analysis was made to correlate the incident laser power and the scatter of the values, it was found that the magnitude of deviation of experimental points is quite independent of the incident power. This observation, together with the "upper-shift" tendency of the experimental points, suggests that the power dependent Brillouin shift does not seem important in the present case. As discussed previously, the experimental data obtained from the high Brillouin components give more coherent results for hypersonic velocity as a function of gas density (Fig. 8). Therefore, this may help to understand the source of the scatter in the first Brillouin results.

The possible origin of the second and higher order SBS components can fall into two types as observed by Korobkin et al[26]. Firstly, they may result from the optical mixing of the original laser light and the Brillouin shifted light; and secondly, they may be produced one at a time but consecutively by the shifted relaxed incident beams. Judging from the interferograms obtained from photographing the incident light and the scatter light simultaneously, it was found that the higher order components in the present case usually fall into the second type. It may then be logically concluded that the second and subsequent incident light produce much more stable SBS shifts than the first. In other words, the initial laser beam entering into the gas medium seems to induce a certain disturbance in the medium to cause the hypersonic velocity to deviate considerably from the adiabatic sound velocity. The exact nature of such a disturbance cannot be easily understood. The possible explanation, however, may come from the better understanding of the breakdown in the gas.

(3) Calculation of the hypersonic speed in O_2 as a function of gas density

For the general property of the frequency dispersion of sound waves in a gas medium, various relaxation processes which are present in the medium have to be considered. Assuming that the contribution of the nontranslation degree of freedom to the specific heat is most important to the relaxation phenomenon, variation of the acoustic velocity on frequency can be considered to depend largely on the vibrational as well as the rotational relaxations in the medium. Since the contribution of the rotational relaxation to the dispersion is negligible for the present sample, only the vibrational relaxation becomes important. Furthermore, it is known that the vibrational specific heat for oxygen gas at room temperature makes a very small contribution to the specific heat. It is therefore justified to apporximate the hypersonic speed by the low frequency speed.

Unlike for the case of argon, no experimental ultrasonic data for oxygen at the present density range is available. In order to compare the present results with the low frequency sound speed, one has to compute it using known relationships. The speed, C_0, for low frequency may be given by[28]

$$C_0^2 = - \frac{\gamma V^2}{M} \left(\frac{\partial P}{\partial V}\right)_T \qquad (3\text{-}10)$$

where γ is the ratio of the specific heat at constant pressure to that at constant volume; M, the gram molecular weight; V, the specific volume; and $\left(\frac{\partial P}{\partial V}\right)_T$, the usual thermodynamic partial derivatives. For

oxygen gas, the values of γ and the quantities of $V^2 \left(\frac{\partial P}{\partial V}\right)_T$ at various densities were obtained from the P-V-T data by Goodwin and Weber[29]. As introduced above, the calculated sound speed is represented in Figs. 7 and 8. The experimental points in Fig. 8 lie somewhat below the calculated curve. A similar discrepancy has been found in the case of CO_2, N_2 and CH_4 by Saito et al[22]. However, the qualitative trend in the relationship seems to agree between the calculated and experimental data.

ACKNOWLEDGEMENTS

The author is grateful to his supervisor, Professor C. W. Cho, for his close guidance, helpful criticisms, and continued encouragement in the course of experiments and during the preparation of the thesis.

The author wishes to thank Dr. N. D. Foltz who provided the guidance in the present experiments, and Dr. R. Tipping for his many stimulated discussions.

The author would also like to express his gratitude to Dr. D. Barton, Department of Chemistry, for the use of his CEC 21-614 Residual Gas Analyzer, which was used to analyze the gas samples. The assistance of Mr. C. T. W. Hsieh in performing the experiments is sincerely appreciated.

The financial support in the form of Departmental Fellowships from Memorial University, which enabled the author to complete this work, is gratefully acknowledged.

REFERENCES

1. P. A. Fleury and R. Y. Chiao, J. Acout. Soc. Am. 39, 751 (1966)
   D. H. Rank, E. M. Kiess, Uwe Fink, and T. A. Wiggins, J. Opt. Soc. Am. 55, 925 (1965)
2. E. Garmire and C. H. Townes, Appl. Phys. Lett. 5, 84 (1964)
3. D. H. Rank, T. A. Wiggins, R. H. Wick, D. P. Eastman, and A. H. Guenther, J. Opt. Soc. 56, 174 (1966)
4. D. I. Mash, V. V. Morozov, V. S. Starunov, and I. L. Fabelinskii, JETP Lett. (English translation) 2, 349 (1965)
5. R. G. Brewer and K. E. Rieckhoff, Phys. Rev. Lett. 14, 334 (1964)
6. E. E. Hagenlocker and W. G. Rado, Appl. Phys. Lett. 7, 236 (1965)
7. D. R. Dietz, C. W. Cho, D. H. Rank, and T. A. Wiggins, Appl. Opt. 8, 1248 (1969)
8. R. M. Herman and M. A. Gray, Phys. Rev. Lett. 19, 824 (1967)
9. D. H. Rank, C. W. Cho, N. D. Foltz, and T. A. Wiggins, Phys. Rev. Lett. 19, 828 (1967)
10. T. A. Wiggins, C. W. Cho, D. R. Dietz, and N. D. Foltz, Phys. Rev. Lett. 20, 831 (1968)
11. D. R. Dietz, M.Sc. Thesis, Pennsylvania State University, University Park, Pennsylvania, U.S.A., Dec. 1968
12. M. A. Gray and R. M. Herman, Phys. Rev. 181, 374 (1969)
13. R. W. Mink and W. G. Rado, J. Appl. Phys. 37, 355 (1966)
14. A. Michels, A. Botzen, and W. Schuurman, Physica, 20, 1144 (1954)
15. International Critical Tables, Vol. III, McGraw-Hill Book Co., Inc., p. 8 (1928)

16. J. L. Delcroix, Plasma Physics, John Wiley & Sons, Ltd., p. 159 (1967)

17. Yu. P. Raizer, JETP (English translation) 21, 1009 (1965)

18. C. Snook, M.Sc. Thesis, Memorial University of Newfoundland, St. John's, Newfoundland, Canada, Sept. 1962

19. M. P. Lallemand and A. Longequeue, Comptes Rendus, Acad. Sc. Paris, t. 269, serié B 1101 (1969)

20. A. Lacam and J. Noury, J. Phys. Radium, 14, 272 (1953)

21. D. J. Mash, V. V. Morozov, V. S. Strarunov, and I. L. Fabelinskii, JETP Lett. (English translation) 28, 1085 (1969)

22. T. T. Saito, L. M. Peterson, D. H. Rank, and T. A. Wiggins, J. Opt. Soc. Am. 60, 749 (1970)

23. International Critical Tables, Vol. VII, McGraw-Hill Book Co., Inc., p. 6 and p. 8 (1928)

24. N. R. Goldblatt and T. A. Litovitz, J. Acous. Soc. Am. 41, 1301 (1967)

25. C. S. Wang, Phys. Rev. Lett. 24, 1394 (1970)

26. V. V. Korobkin, D. I. Mash, V. V. Morozov, I. L. Fabelinskii, and Y. Shchelev, JETP Lett. 5, 372 (1967)

27. H. O. Kneser, Physical Acoustics, Vol. II, edit. by Mason, W. P., Academic Press (1965)

28. J. O. Hirschfelder, C. F. Curties, and R. B. Bird, Molecular theory of gases and liquids, John Wiley & Sons, Ltd., p. 232 (1954)

29. R. D. Goodwin and L. A. Weber, J. Res. NBS 73A (Phys. and Chem.) No. 1, 15 (1969)